



An experimental and mechanistic study on the laminar flame speed, Markstein length and flame chemistry of the butanol isomers



Fujia Wu, Chung K. Law*

Department of Mechanical and Aerospace Engineering, Princeton University, Princeton, NJ 08544, USA

ARTICLE INFO

Article history:

Received 7 November 2012

Received in revised form 25 May 2013

Accepted 12 June 2013

Available online 16 July 2013

Keywords:

Laminar flame speeds

Butanol isomers

Flame chemistry

Markstein lengths

ABSTRACT

Laminar flame speeds and Markstein lengths for *n*-butanol, *s*-butanol, *i*-butanol and *t*-butanol at pressures from 1 to 5 atm were experimentally measured in a heated, dual-chamber vessel. Results at all pressures show that *n*-butanol has the highest flame speeds, followed by *s*-butanol and *i*-butanol, and then *t*-butanol. Results further show that the reduced Markstein length measured for *n*-butanol as compared to other isomers is a flame thickness effect, and that all four isomers have similar Markstein numbers, which is the appropriate nondimensional parameter to quantify flame stretch. Computation and flame chemistry analysis were performed using two recently published kinetic models on butanol isomers by Sarathy et al. and Ranzi et al., respectively. Comparison shows the former model satisfactorily agrees with the present results while agreement of the latter is less satisfactory. Based on reaction path analysis the major differences of the two models on fuel cracking pathway were identified. It is concluded that the primary reason for the lowered flame speed of *s*-butanol, *i*-butanol and *t*-butanol is that they crack into more branched intermediate species which are relatively stable, such as *iso*-butene, *iso*-propenol and acetone. This indicates that the general rule that fuel branching reduces flame speed for hydrocarbons can also be applied to alcohols, and that the fundamental reason for this generality is that in alcohols C—O has similar bond energy to the C—C bond while O—H has similar bond energy to the C—H bond.

© 2013 The Combustion Institute. Published by Elsevier Inc. All rights reserved.

1. Introduction

Butanol holds much potential as a significant alternative transportation fuel. Compared to methanol and ethanol, butanol not only has a diverse source of feedstock, but it also has more desirable fuel properties such as higher energy density, miscibility with gasoline and diesel, and less corrosion. In order to evaluate and implement butanol as a practical transportation fuel, it is therefore important to understand its combustion characteristics.

There are four butanol isomers, namely normal butanol (*n*-butanol or 1-butanol), secondary butanol (*s*-butanol or 2-butanol), isobutanol (*i*-butanol) and tertiary butanol (*t*-butanol). Most previous studies have focused on *n*-butanol, with *s*-butanol, *i*-butanol and *t*-butanol receiving considerably less attention. It is noted [1] that *s*-butanol and *i*-butanol are also produced in biological fermentation processes, and that *t*-butanol is a petrochemical product which has been used for decades as an octane enhancer in gasoline. Therefore studying the combustion characteristics of all the four butanol isomers is useful and important.

The laminar flame speed of a combustible mixture is an important global combustion parameter which also contains the chemical information of the mixture such that it can be used to partially

validate chemical kinetics models developed for the mixture. For the butanol isomers, not many data other than those of *n*-butanol have been reported, and most of the measurements were conducted only at atmospheric pressure. Specifically, laminar flame speeds were reported by Sarathy et al. [2] for *n*-butanol at 0.89 atm pressure and initial temperature of 350 K; by Veloo and Egolfopoulos [3] for the four isomers at 1 atm and 343 K; by Liu et al. [4] for *n*-butanol and *i*-butanol at 1 atm and 2 atm and initial temperature of 353 K; and by Gu et al. [5–8] for *n*-butanol from 1 atm to 2.5 atm, *t*-butanol from 1 atm to 5 atm, and stoichiometric mixtures of the four isomers with air up to 7.5 atm, all at the initial temperature of 425 K.

A primary objective of the present flame speed measurements is to aid in the development and validation of detailed chemical kinetic models. Considerable effort has been devoted to model development of *n*-butanol [9–12], while models for other butanol isomers were also subsequently proposed. Van Geem et al. presented a high-temperature model for *n*-butanol, *s*-butanol and *t*-butanol [13], and Moss et al. presented an automatically generated mechanism for all four butanol isomers [14]. Recently Sarathy et al. published a detailed model for all four butanol isomers [15], and Ranzi et al. also published an alcohol mechanism that includes the butanol isomers [16].

The present investigation aims to first acquire additional data on the laminar flame speed and the associated Markstein length

* Corresponding author.

E-mail address: cklaw@princeton.edu (C.K. Law).

for all the butanol isomers at atmospheric and elevated pressures. By using expanding spherical flames, we have subsequently measured the laminar flame speeds of *n*-butanol, *s*-butanol, *i*-butanol and *t*-butanol at 1, 2 and 5 atm and at elevated initial temperatures. These data can be used for validating and developing the kinetic mechanism for the butanol isomers. In particular, since the present investigation yields validation data sets for all the isomers across a wide range of identical experimental conditions, we have conducted a consistent comparison of the reactivity among them, yielding valuable insight into the controlling kinetics.

2. Methodology

2.1. Experimental setup

Since detailed specification of the experimental apparatus, procedure and data analysis were reported in previous publications [17–19], only a brief description is provided here. The apparatus consists of a cylindrical chamber radially situated within another cylindrical chamber of substantially larger volume. The wall of the inner chamber is fitted with a series of holes that can be mechanically opened and closed to allow the union and separation of the gases. The desired equivalence ratio in the inner chamber is obtained by monitoring the partial pressures of the gases in the inner chamber. The outer chamber is filled with a mixture of inert gases to match the pressure and density of the gas in the inner chamber. Spark ignition and opening the holes between the inner and outer chambers occur concurrently, resulting in an expanding spherical flame that propagates throughout the inner chamber in essentially an isobaric environment. The outer chamber is covered with silicon electrical heaters, hence enabling it to act as an oven to uniformly heat the inner chamber to a given temperature. The flame surface is visualized using a pin-hole Schlieren system coupled to a high-speed camera.

Tracking the flamefront yields the history of the radius of the spherical flame as a function of time. For extrapolation of the laminar flame speed, we employ the nonlinear relation of Kelley et al. [20],

$$S_b^0 t + C = r_f + 2L_b \ln r_f - \frac{4L_b^2}{r_f} - \frac{8L_b^3}{3r_f^2} \quad (1)$$

where S_b^0 is the adiabatic, unstretched gas speed of the burned mixture relative to the flame, r_f the flame radius, L_b the Markstein length at the burned mixture side and t the time. Eq. (1) contains

up to the third-order accuracy in terms of the inverse flame radius. Once S_b^0 is measured, the laminar flame speed (flame velocity relative to the unburned gas) S_b^0 is calculated based on the continuity relation,

$$S_b^0 \rho_b = S_u^0 \rho_u \quad (2)$$

where ρ_u and ρ_b are densities of the unburned gas mixture and equilibrium burnt gas mixture, respectively. For flame speed measurements using expanding spherical flames, the data selected for extrapolation need to be within a certain radius range in that the small and large radius data are respectively affected by the influence of ignition and the chamber confinement, as discussed in details in Refs. [21–24]. For our experimental setup and the fuels studied, a conservative assessment of this range is between radii of 1.0–1.8 cm for most cases. For flames with very large Lewis number, the lower bound needs to further increase to eliminate the enhanced influence of ignition at such conditions. Based on the response of the extrapolation result to the selection of lower and upper bonds, we estimate the uncertainty of the flame speed is approximately ± 2 cm/s. Besides flame speed, the reported equivalence ratio also has uncertainty. We found that the error in the equivalence ratio primarily results from the error in the oxidizer concentration in the oxidizer/air mixture and the error in the pressure gauge readings. Based on the two errors, the uncertainty of the equivalence ratio is estimated to be $\pm 2\%$. Table 1 contains the pertinent information of the fuels considered in the current investigation.

2.2. Numerical approach

In the present work, we used the kinetic mechanisms of Sarathy et al. [15] and Ranzi et al. [16] for comparison and analysis, for the following reasons: (1) Both models were developed recently; (2) Both models cover all four butanol isomers, thus allowing a consistent comparison for all butanol isomers; (3) Both models include transport data needed by flame simulations. For ease of referencing we shall designate these two reaction mechanisms as the S-mechanism [15] and the R-mechanism [16], respectively.

The computation with the S-mechanism used the high-temperature version of the model, with 284 species and 1892 reactions consisting of the high-temperature reaction classes [15], such as H-abstraction, fuel radical decomposition, isomerization and tautomerization. These reactions dominate fuel oxidization when there is a high-temperature radical pool such as H, OH, O and CH₃. For 1-D planar flames, since there is always back diffusion

Table 1
Fuel specific properties.

Chemical name	Molecular formula	Structure	Purity
<i>n</i> -Butanol (1-butanol)	C ₄ H ₉ OH		99 + %
<i>s</i> -Butanol (2-butanol)	C ₄ H ₉ OH		99 + %
<i>i</i> -Butanol (<i>iso</i> -butanol)	C ₄ H ₉ OH		99 + %
<i>t</i> -Butanol (<i>tert</i> -butanol)	C ₄ H ₉ OH		99 + %

of the radicals from the active reaction zone towards the unburned mixture, these reactions are adequate enough for the simulation of laminar flame speeds. The calculations with the S-mechanism were performed by Chemkin II PREMIX Program [25]. Since the mechanism includes pressure dependent reactions with rate constants formulated by the PLOG function which is not accepted by Chemkin II, we used the modified Chemkin II interpreter and library developed by Gou et al. [26], which implements the PLOG formulation for pressure-dependent reactions.

The R-mechanism includes semi-detailed reactions. The full mechanism includes the chemistry of hydrocarbon up to C₁₆, alcohols and esters, etc. In the present computation, we used a sub-model of it that includes only the chemistry of C₁–C₆ hydrocarbons and alcohols, consisting of 249 species and 7933 reactions. The R-mechanism is not Chemkin II compatible because of the non-integer coefficients of some semi-detailed reactions. The computations were conducted by Open SMOKE code [27]. Both PREMIX and Open SMOKE solve the same set of governing equations described in [25], i.e., the one-dimensional, steady, planar flames.

Calculations using both programs employed mixture-averaged transport formulation, Soret diffusion, and incorporated adaptive gridding, which was refined until a grid-independent solution was found. For PREMIX, the calculations have approximately 250 grid points (GRAD 0.1, CURV 0.1).

3. Results

3.1. Laminar flame speeds

The measured flame speeds at 1, 2 and 5 atm are plotted with symbols (circles, squares, etc.) in Fig. 1. For all the isomers, measurements at 1 and 2 atm were conducted with initial gas temperature of 353 K and standard synthesized air as oxidizer. Experimentation at higher pressures was however limited by fuel condensation as more fuel vapor is needed. To circumvent this difficulty, we chose the initial gas temperature to be 373 K, and used an oxidizer with reduced oxygen concentration and a mixture of argon and helium as bath gas (O₂%:Ar%:He% = 13%:38.1%:48.9% by mole). This renders the fuel vapor pressure as low as possible while the mixture also has a favorable effective Lewis number for accurate extrapolation, noting that using pure argon or helium as bath gas will cause the Lewis number to be either too small or too large. With these provisions, we were able to acquire data up to 5 atm.

From Fig. 1 it is seen that n-butanol has the highest flame speeds at all pressures, followed by s-butanol and i-butanol, and then t-butanol which has the lowest flame speeds. The experiments indicate that the flame speed difference between s-butanol and i-butanol is only 1% for all conditions, which is less than the experiment uncertainty. The flame speed difference between n-butanol and i-butanol (or s-butanol) is 7% at 1 atm and 11% at 5 atm, while the difference between n-butanol and t-butanol is 22% at 1 atm and 32% at 5 atm. The present experiment shows the following trend for the flame speeds of the four butanols: n-butanol > s-butanol ≈ i-butanol > t-butanol. This trend remains the same as pressure increases from 1 to 5 atm.

We next discuss the comparison of the present measurements with previously reported measurements and kinetic model predictions. For previous measurements, we consider the flame speeds of n-butanol and i-butanol at 1–2 atm reported by Liu et al. [4] and the flame speeds of all four isomers at 1 atm reported by Veloo and Egolfopoulos [3]. The data by Liu et al. [4] were obtained using the same vessel as the present work. The data by Veloo and Egolfopoulos [3] were obtained using the counterflow flame at unburned gas temperature of 343 K. Direct comparison with Veloo and Egolfopoulos [3] is not possible due to the 10 K difference in unburned gas temperature. Nevertheless, in Figs. 2–5 we plot both

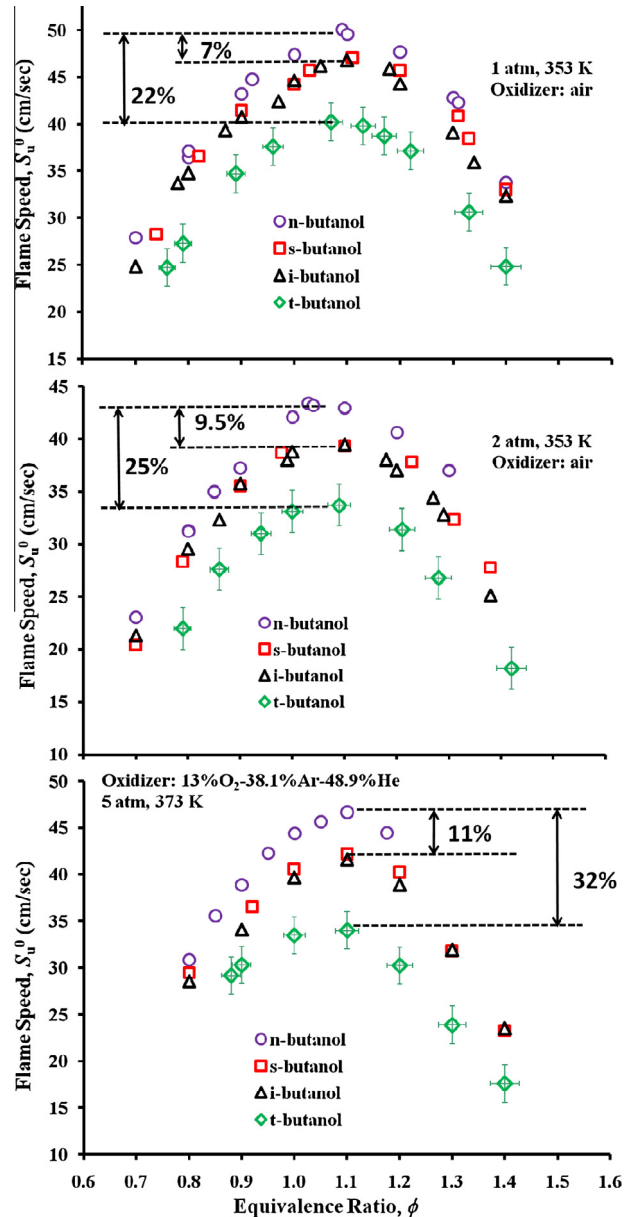


Fig. 1. Measured flame speeds, S_u^0 , of butanol isomers at 1, 2 and 5 atm. Error bars are plotted only on the data for t-butanol for clarity.

the original data of Veloo and Egolfopoulos [3] and an empirical correction of them based on $S_u^0 \sim T_u^{1.8}$ to account for the 10 K difference in unburned gas temperature. The correction results in 1–2 cm/s increase in flame speed. We note that the relation $S_u^0 \sim T_u^{1.8}$ is not meant to be general. Instead, it simply provides a local approximation to give an estimate of the effect of the 10 K difference in the unburned gas temperature. Using the computed values of flame speed at 343 K with the S-mechanism, we found that around 353 K this power index is between 1.7 and 2.2 for all four butanol isomers. For comparison with model predictions, we consider the S- and R-mechanisms.

Figure 2 compares the present results at 1 and 2 atm with measurements by Liu et al. [4] and by Veloo and Egolfopoulos [3] as well as the model predictions by the S- and R-mechanisms. We first see that the present results for n-butanol and i-butanol agree well with those of Liu et al. [4]. The two sets of data are almost identical for most of the conditions. At the very rich conditions for i-butanol, the present data is slightly higher than those of Liu et al. [4]; however, the difference is within the uncertainty band.

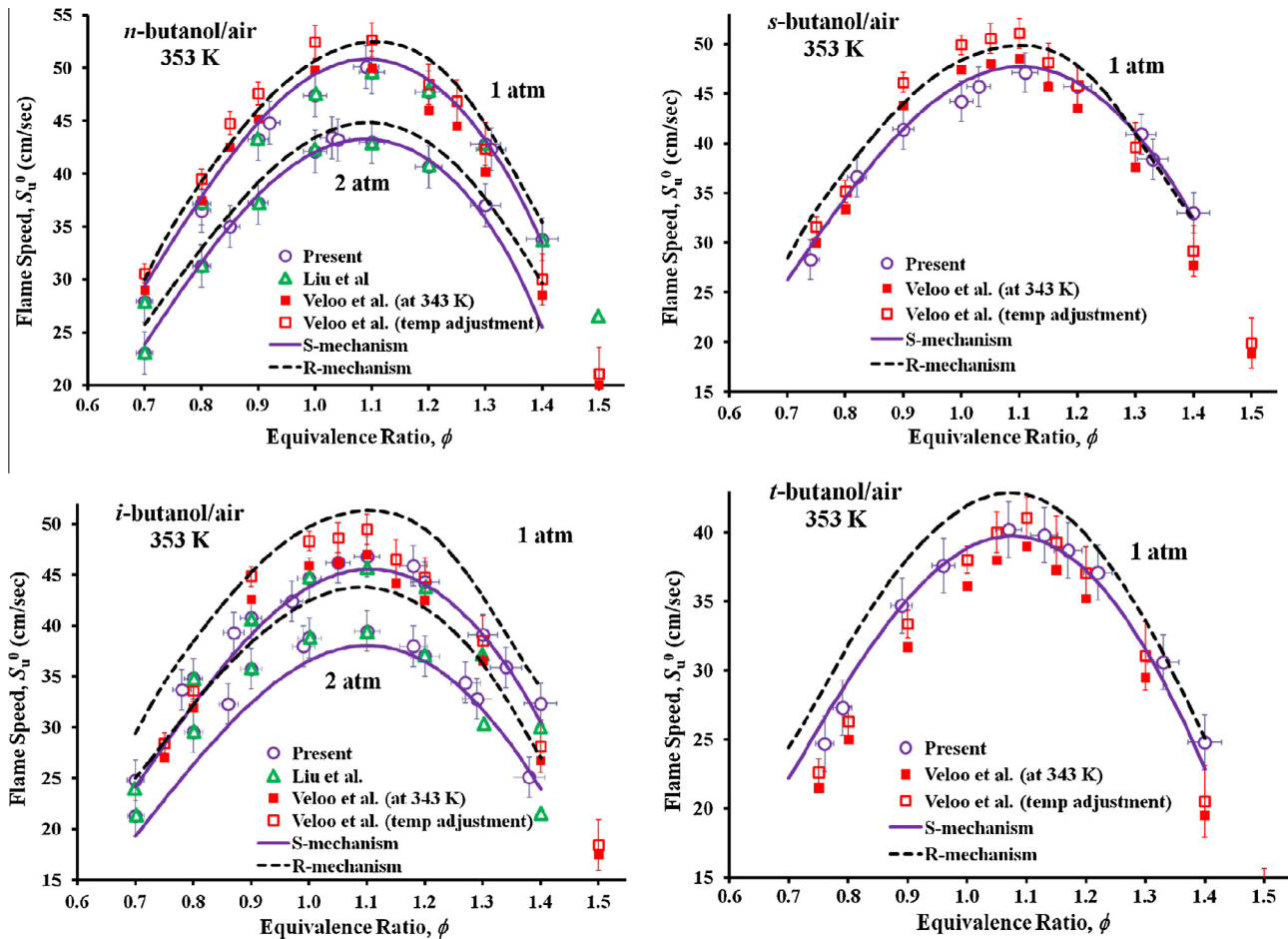


Fig. 2. The present results at 1 and 2 atm compared with measurements by Liu et al. [4] and by Veloo and Egolfopoulos [3] as well as the model predictions by the S- and R-mechanisms.

Comparing the present data with those of Veloo and Egolfopoulos [3], we see that the two data sets are close for *n*-butanol, *s*-butanol and *i*-butanol. However, this does not suggest agreement because the data by Veloo and Egolfopoulos [3] were obtained at unburned gas temperature 10 K lower. If the present is compared against the temperature-adjusted data of Veloo and Egolfopoulos [3], then the present data are lower by up to 8% at $\phi < 1.2$ and slightly higher at $\phi > 1.3$. In addition, the peak flame speed for the data of Veloo and Egolfopoulos [3] is at $\phi \approx 1.05$, while the calculations and the present measurements peak around $\phi \approx 1.1$. This shifting in equivalence ratio was also observed in previous measurements on other liquid fuels between counterflow flames and spherical flames [18,19,28–30]. Finally, despite the difference for *n*-butanol, *s*-butanol and *i*-butanol, the present results on *t*-butanol agree well with those by Veloo and Egolfopoulos [3] after temperature adjustment.

Gu et al. [6] also reported flame speeds for butanol isomers up to 0.75 MPa at $\phi = 1.0$. The measurements were conducted at an unburned gas temperature of 428 K, a direct comparison with the present results is also not possible. However, it is noted that the trend of their flame speed for different butanol isomers varies as pressure increases, *i.e.*, compared to *n*-butanol, the flame speed of *s*-butanol and *i*-butanol are lower by 13% at 1 atm, but higher by 11% at 0.5 MPa and 0.75 MPa. This reversal in trend as pressure increases is not observed in the present measurements.

We next compare results from different models. Figures 3 and 4 plot the present results compared with model predictions of the S- and R-mechanisms, respectively, for all isomers. Figure 3 shows an overall satisfactory agreement with the S-mechanism for all fuels

at all pressures. In particular, the model prediction falls well within the uncertainty band of the present experimental data for all conditions except for *s*-butanol at 5 atm and *i*-butanol at 2 atm, where a slight over and under prediction is seen, respectively. In addition, the model shows that the flame speed of *s*-butanol is 5–9% higher than that of *i*-butanol, while the experiment yields almost the same flame speed for the two fuels.

Figure 4 shows overall less satisfactory agreement with the R-mechanism. For *n*-butanol and *s*-butanol, the predictions are slightly above the uncertainty upper limit of the present data at 1 and 2 atm, whereas at 5 atm the predictions are slightly below the uncertainty lower limit. For *i*-butanol and *t*-butanol, the predictions are above the uncertainty upper limit at 1 and 2 atm, but fall within the uncertainty band at 5 atm. In other words, as pressure increases, the model performance changes from over prediction to under prediction (for *n*-butanol and *s*-butanol) and agreement (for *i*-butanol and *t*-butanol). In addition, the predictions indicate that the flame speed of *i*-butanol is 3–4% higher than that of *s*-butanol, which is opposite to the predictions of the S-mechanism, while the experiment show *i*-butanol and *s*-butanol have almost the same flame speed.

3.2. Markstein lengths

Figure 5 plots the Markstein lengths at the burned side, L_b in Eq. (1), corresponding to the laminar flame speed measurements shown in Fig. 1. This value directly results from the extrapolation using Eq. (1). It is seen that the Markstein lengths of all the butanol isomers have similar values at 1 and 2 atm and with air as the

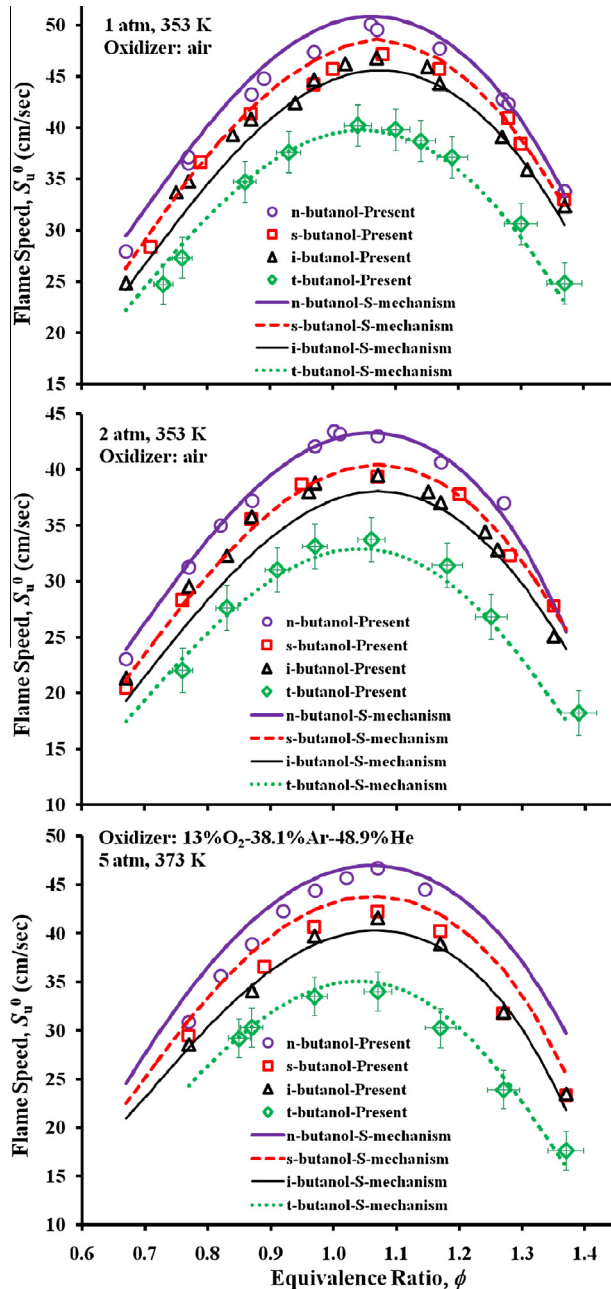


Fig. 3. Comparison of the present results at 1, 2 and 5 atm with the model predictions by the S-mechanism.

oxidizer, with differences smaller than the experimental uncertainty. However, at 5 atm and with an oxygen–helium–argon mixture as the oxidizer, the Markstein lengths of *n*-butanol are considerably lower than those of the other three isomers.

To reconcile the above difference, we first note that since the Markstein length is a dimensional quantity, it may not be appropriate to extract the underlying physical information through quantitative comparison of its values obtained from different situations. Indeed, the relevant parameter that characterizes the sensitivity of flame speed to stretch is the Markstein number, which is the Markstein length scaled by the flame thickness. Since the 5 atm experiments were conducted using different inert, and since the flame thickness also decreases with increasing pressure, in order to eliminate the flame thickness effect it is necessary to perform the comparison on the basis of the Markstein number instead of

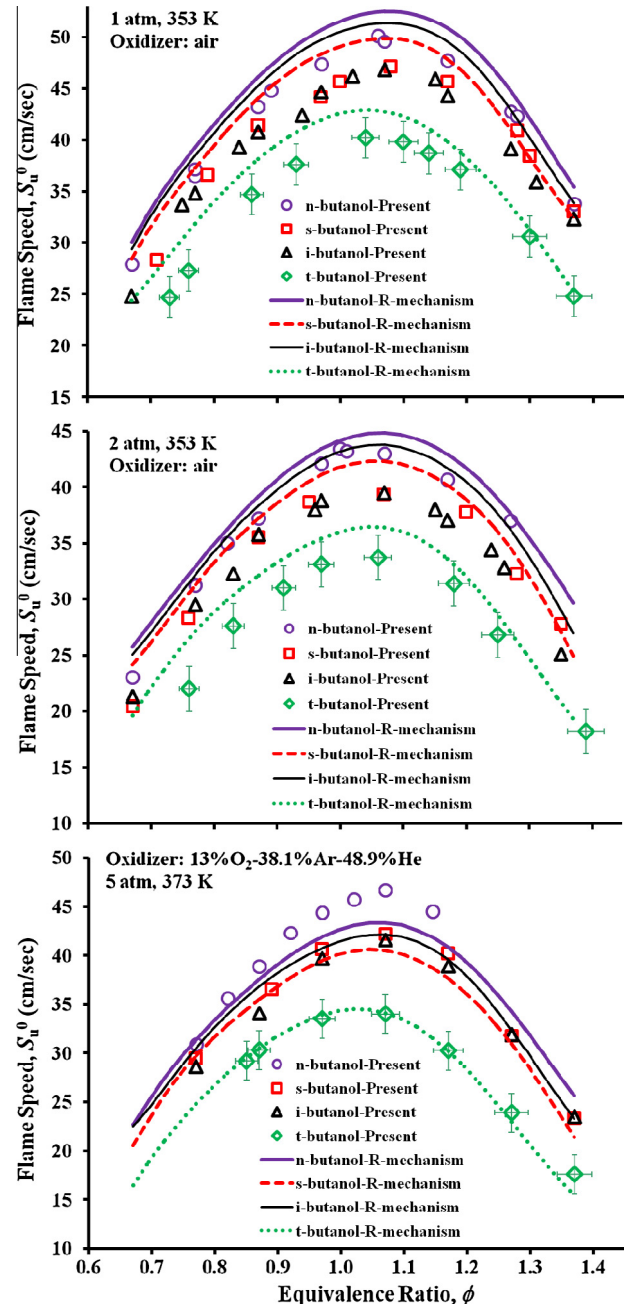


Fig. 4. Comparison of the present results at 1, 2 and 5 atm with the model predictions by the R-mechanism.

the Markstein length. **Figure 6** therefore plots the Markstein numbers for the isomers, with the flame thickness δ_L evaluated using the gradient method, with the temperature profile calculated by Premix and the S-mechanism,

$$\delta_L = \frac{T_{ad} - T_u}{(dT/dx)_{\max}} \quad (3)$$

where T_{ad} is the adiabatic flame temperature, T_u the unburned mixture temperature, and the subscript “max” indicates the maximum value in the computation domain. It is then seen that the Markstein numbers of *n*-butanol at 5 atm and with an oxygen–helium–argon mixture as the oxidizer are almost the same as those of the other isomers. This indicates that the smaller Markstein length for *n*-butanol is caused by its smaller flame thickness as compared to

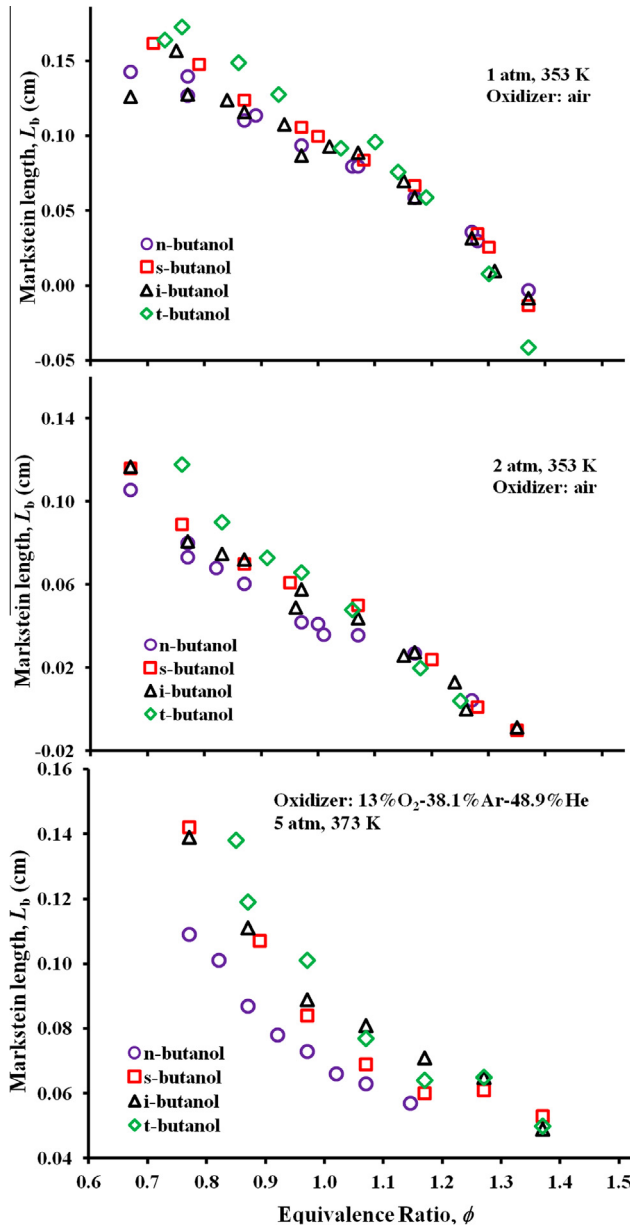


Fig. 5. Measured Markstein lengths, L_b , of butanol isomers at 1, 2 and 5 atm.

the other isomers. From Fig. 6 it is also seen that the four isomers also have similar Markstein numbers at 1 atm and 2 atm with air as oxidizer. Consequently, despite the isomers having distinct flame speeds, the effects of their transport characteristics on the global combustion parameters are similar.

4. Discussions

4.1. Thermal effects

We shall next endeavor to identify the fundamental reasons governing ordering of the laminar flame speeds among the isomers. From flame theory, the laminar flame speed is determined by three aspects of the mixture: namely thermal, transport and kinetic effects. Figures 5 and 6 show that all four isomers have similar transport effects as they have similar Markstein numbers. We shall therefore investigate the thermal and kinetic effects.

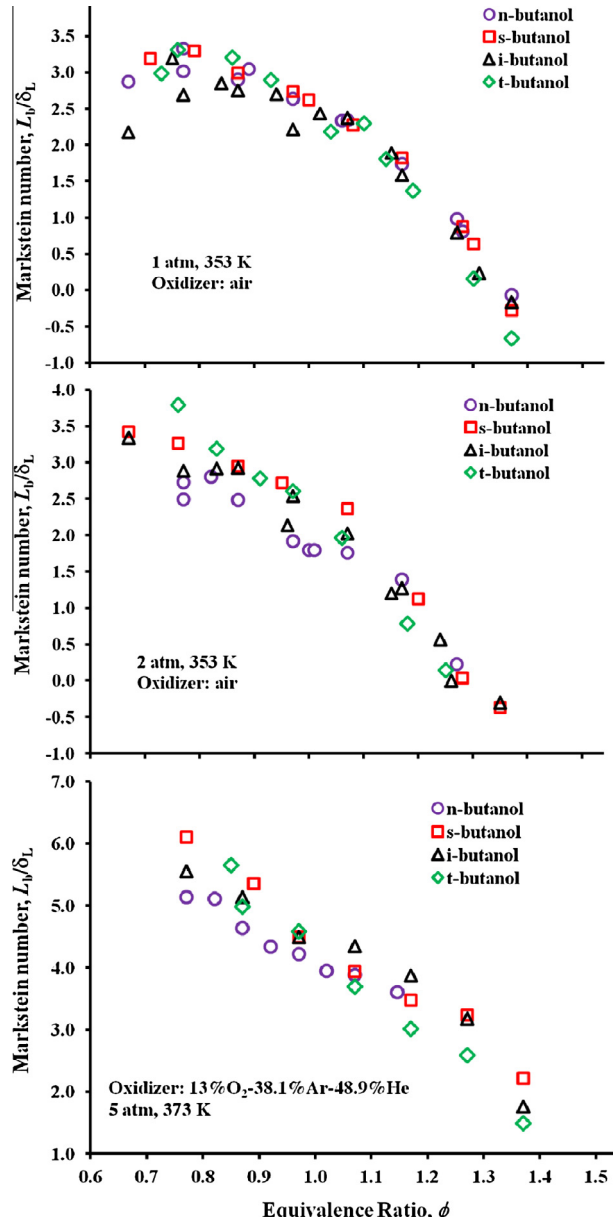


Fig. 6. Measured Markstein numbers, L_b/δ_L , of butanol isomers at 1, 2 and 5 atm.

Figure 7 plots the adiabatic flame temperatures of the four isomers at 1 and 5 atm. It is seen that *n*-butanol has the highest adiabatic flame temperature, followed by *s*-butanol, *i*-butanol and then *t*-butanol. However, the differences among them are small. Specifically, the difference between *t*-butanol and *n*-butanol is around 20 K at lean and stoichiometric conditions and around 30 K on the rich side. To quantify the effect of such a difference, additional cases were calculated for *t*-butanol/air at 1 atm with the adiabatic flame temperature increased to that of *n*-butanol/air by slightly reducing the nitrogen concentration. The calculated results are plotted in Fig. 8. It is seen that the increase in the flame speed by this temperature adjustment is about 2 cm/sec, which is only 1/5 of the difference between the calculated flame speeds of *n*-butanol and *t*-butanol. This indicates that flame temperature is not the main reason for the flame speed difference among the isomers.

Figures 9 and 10 plot the temperature and heat release profiles of the one-dimensional planar flames for the isomers at 1 and 5 atm, calculated by using the S- and R-mechanisms, respectively.

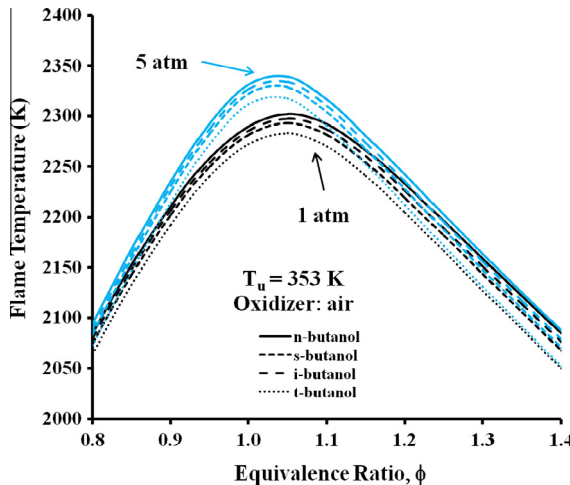


Fig. 7. Computed temperature and heat release profiles of 1-D planar flame for the butanol isomers.

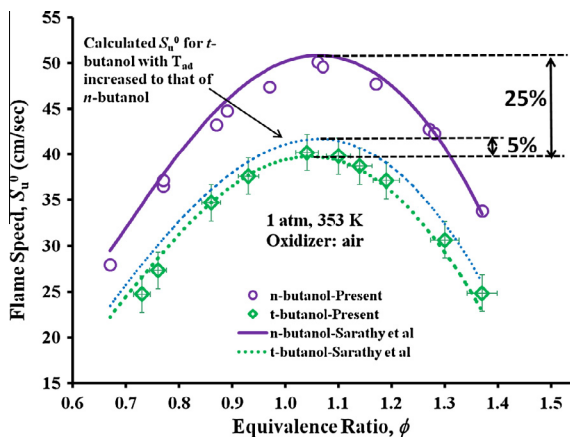


Fig. 8. Computed flame speed of t-butanol/ N_2/O_2 mixture with adiabatic flame temperature increased to that of n-butanol/air by reducing nitrogen concentration. Measured and computed flame speeds of n-butanol/air and t-butanol/air are plotted for comparison.

It is seen from both figures that the flame temperatures upstream and downstream of the flame zone for the four flames are almost identical while they differ significantly within the flame zone. This means that the total heat release is the same for all fuels while the heat release rate differs. It again indicates that the flame speed difference among the butanol isomers is not purely a thermal effect. From Figs. 9 and 10, it is seen that with the S-mechanism, n-butanol has the highest heat release rate, followed by s-butanol, i-butanol and then t-butanol; while with the R-mechanism, n-butanol has the highest heat release rate, followed by i-butanol, s-butanol and then t-butanol. The different ordering in the heat release profiles calculated with both mechanisms is consistent with their different predictions of the laminar flame speed. In addition, we find that with both mechanisms as pressure increases from 1 atm to 5 atm the difference among the heat release rates of different isomers also increases. This is also consistent with the pressure effect on the laminar flame speed.

4.2. Sensitivity analysis

To investigate the kinetic effects, we first conduct sensitivity analysis of the rate constants, recognizing that reactions with high

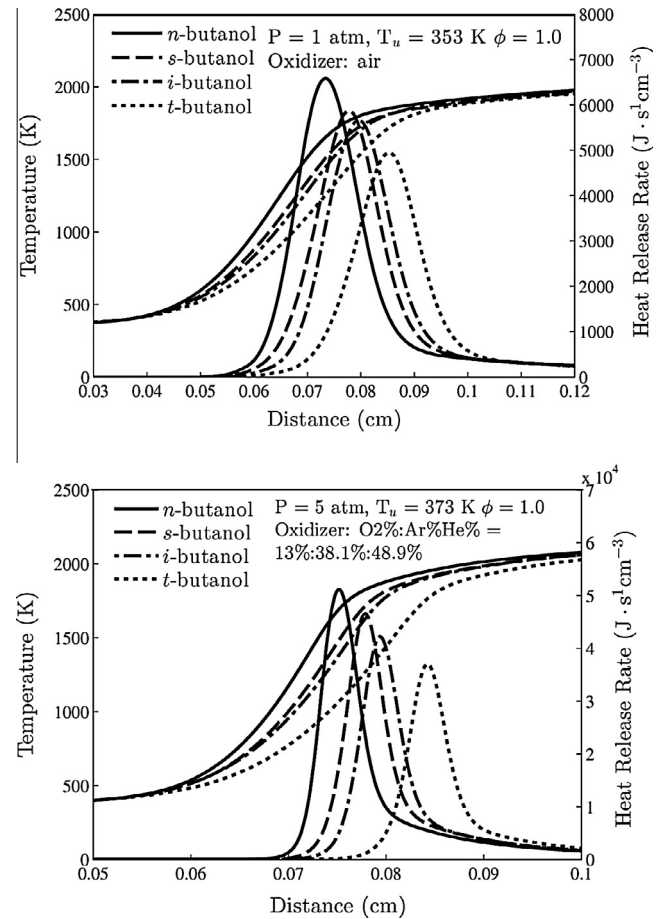


Fig. 9. Computed temperature and heat release profiles of $\phi = 1.0$ 1-D planar flame for the butanol isomers at 1 and 5 atm using the S-mechanism.

sensitivity on the flame speed are rate limiting. The normalized sensitivity coefficient k_i of a reaction i is defined as,

$$k_i = \frac{A_i}{S_u^0} \frac{\partial S_u^0}{\partial A_i} \quad (4)$$

where A_i is the pre-exponential factor of reaction i .

Figures 11 and 12 plot the normalized rate constant sensitivity coefficients for all isomers at 1 atm and 5 atm of the simulations using the S- and R-mechanisms, respectively. First, it is seen that in all cases for all isomers, the flame speed is most sensitive to the kinetics of hydrogen, carbon monoxide, and the small hydrocarbons. The fuel specific reactions are not rate limiting except for a few reactions for t-butanol. This heightened sensitivity on hydrogen and small hydrocarbon kinetics is similar to many other heavy hydrocarbons [18,19,31], indicating that there is no fundamental difference between the kinetics of butanol isomers including t-butanol with that of the other heavy hydrocarbons. For t-butanol the reaction $i-C_4H_8 = i-C_4H_8 + H_2$ shows a small sensitivity at 1 atm in the S-mechanism, and the t-butanol decomposition reactions show noticeable sensitivity at 5 atm in the S-mechanism and at both 1 and 5 atm in the R-mechanism. This indicates the uniqueness of t-butanol kinetics.

Comparing the two mechanisms, it is seen that the H_2 and C_1-C_2 reactions from the sensitivity analysis are largely the same for the two mechanisms, although they might have different sensitivity coefficients. The reactions $C_3H_6 = aC_3H_5 + H$ and $C_3H_6 + OH = aC_3H_5 + H_2O$ show some sensitivity in the S-mechanism, especially

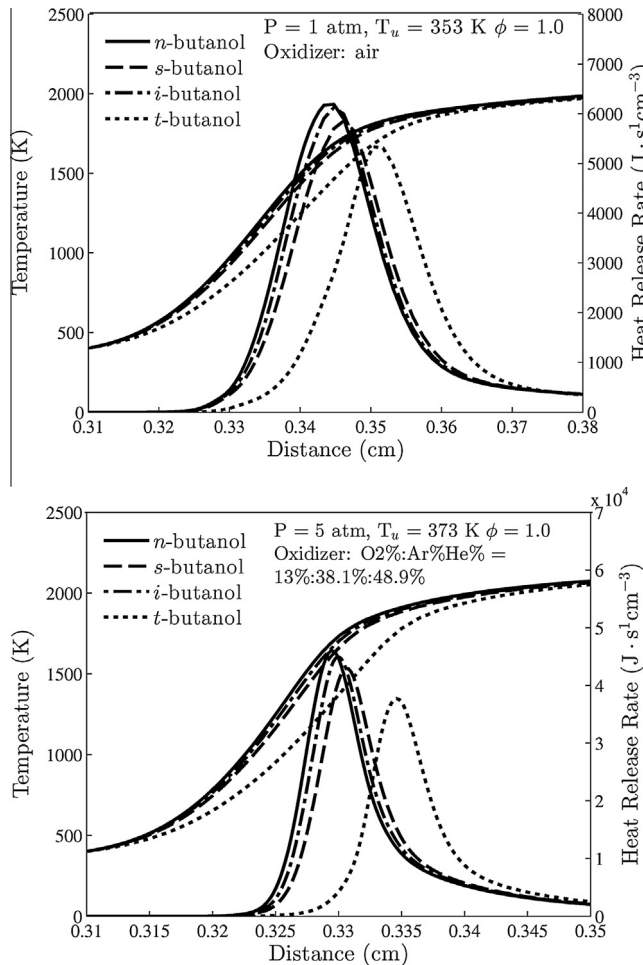


Fig. 10. Computed temperature and heat release profiles of $\phi = 1.0$ 1-D planar flame for the butanol isomers at 1 and 5 atm using the R-mechanism.

for *i*-butanol and *t*-butanol; however, they do not have high sensitivity coefficients in the R-mechanism.

Finally, from the sensitivity analysis we do not see a strong pressure effect from 1 atm to 5 atm. The reactions with high sensitivity coefficients remain largely the same. Since third body reactions (+M) and reactions involving peroxide radicals (e.g. HO_2) are expected to become more sensitive at higher pressures, it is nevertheless noted that such trends are not observed in Figs. 11 and 12. To investigate the cause of this pressure insensitivity, we first recognize that 5 atm is still relatively low, and that the inert we use at such conditions are argon and helium, instead of nitrogen. Thus to assess the high pressure and inert effects, using the S-mechanism we have computed and plot in Fig. 13 the sensitivity coefficients of some representative third body reactions and reactions involving HO_2 for *n*-butanol at higher pressures, with air as the oxidizer. As expected, when the pressure increases from 1 atm to 20 atm, the magnitudes of the sensitivity coefficients of these reactions increase significantly, indicating the importance of third body reactions and peroxide radicals at higher pressures. On the other hand, at 5 atm using $\text{O}_2/\text{Ar}/\text{He}$ mixture as oxidizer these reactions do not show much sensitivity, primarily because the pressure is not high enough. In addition, for the reaction $\text{H} + \text{O}_2 + \text{M} = \text{HO}_2 + \text{M}$, we see that at 5 atm using $\text{O}_2/\text{Ar}/\text{He}$ mixture as oxidizer it has lower sensitivity than using air as the oxidizer. This means that using Ar/He as the inert reduces the importance of third body reactions.

4.3. Reaction path analysis

From the sensitivity analysis, it is seen that it is the oxidation of small fuel fragments that controls the total heat release and therefore the flame propagation. This means that the initial fuel cracking reactions are relatively fast and are not controlling the global rate. Such a rationale was previously suggested in the studies of flame propagation of $\text{C}_5\text{--C}_{12}$ hydrocarbon fuels [18,19,28,32]. Then the question is why the flame speeds of butanol isomers are different.

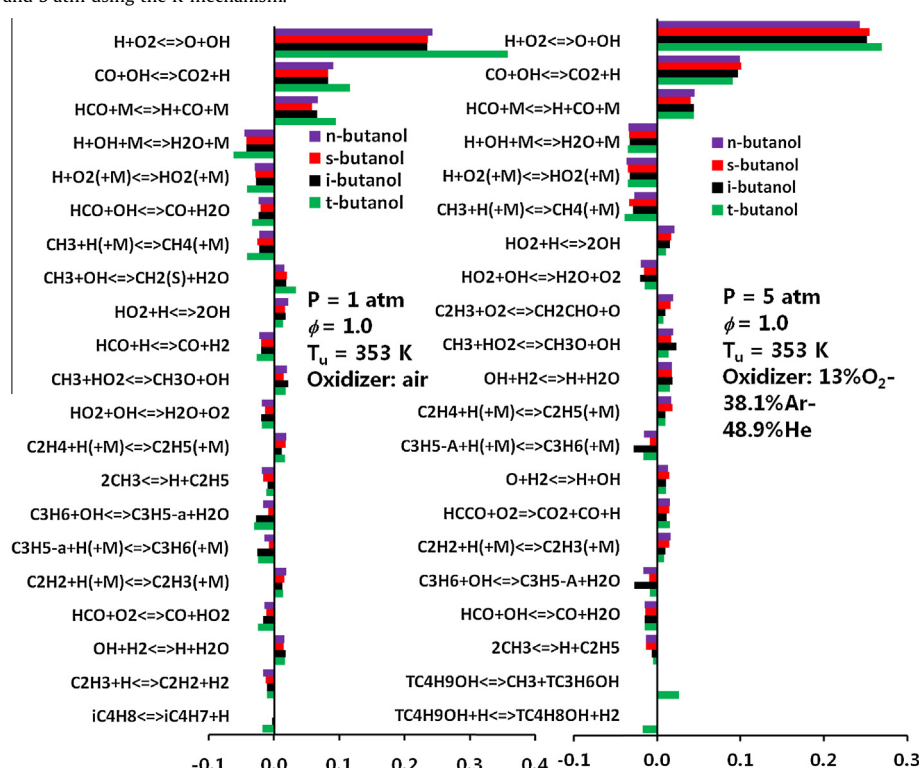


Fig. 11. Normalized rate constant sensitivity coefficients k_i on the flame speed of the $\phi = 1.0$ 1-D planar flame for the butanol isomers at 1 and 5 atm using the S-mechanism.

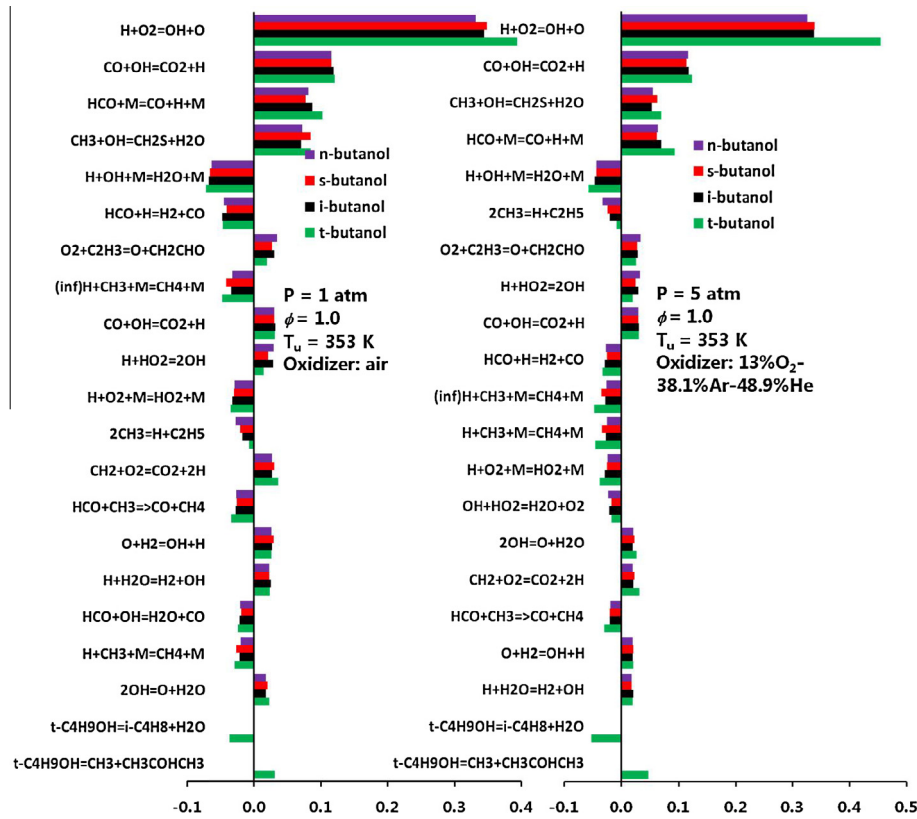


Fig. 12. Normalized rate sensitivity coefficients k_i on the flame speed of the $\phi = 1.0$ 1-D planar flame for the butanol isomers at 1 and 5 atm using the R-mechanism.

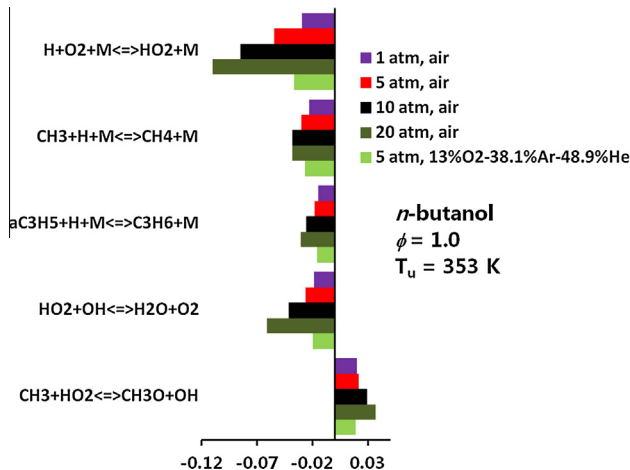


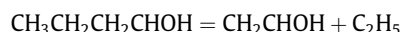
Fig. 13. Normalized rate constant sensitivity coefficients of some representative third body reactions and reactions involving HO_2 for $\phi = 1.0$ 1-D planar *n*-butanol flames at higher pressure with air as oxidizer using the S-mechanism.

The reason lies in the fact that although the fuel-specific reactions are not the rate-limiting steps, they are completely different reactions due to the different molecular structure of the butanol isomers. These fuel specific reactions produce different fuel fragments, and therefore the distributions of intermediate species in the flames of different isomers are different. The reactivity of the intermediate species is different which finally leads to different global heat release.

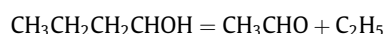
To confirm this explanation, we performed reaction path analysis of the initial fuel cracking process up to a few reaction steps. Figures 14–17 plot the initial fuel cracking reaction paths in the

1-D planar flames for all four isomers, respectively. To investigate the pressure effect and compare the difference between the S- and R-mechanisms, the conversion rates were calculated at 1 and 5 atm in Figs. 14–17. It is seen that for each fuel, the main initial fuel cracking path is the H-abstraction reaction, forming various hydroxybutyl radicals which further crack into smaller species mostly following the β -scission rule, while there are also unimolecular fuel decomposition, fuel radical isomerization and enol-keto tautomerization reactions involved in the initial fuel cracking process.

From Fig. 14, it is seen that for *n*-butanol, the H abstraction reactions convert large percentage of fuel into four hydroxybutyl radicals and small portion of fuel into the *n*-butoxy radical. These five fuel radicals further decompose into smaller fragments, including alkenes, enols, aldehydes and ketones. All fuel radical decompositions almost follow the β -scission rule and most of them occur at the β C–C bond and β C–O bond. Isomerization reactions between fuel radicals can also occur, for example between 4-hydroxybutyl and *n*-butoxy. The fuel molecule can also directly decompose into smaller radical or produce butene via the water elimination reaction. Comparing the two mechanisms, we find that there are two major differences. First, in the R-mechanism any enols produced from the fuel β -scission reactions are replaced by aldehydes or ketones. For example, for 1-hydroxybutyl radical the dominant pathway in the S-mechanism:



which produces ethenol, while in the R-mechanism the dominant pathway is:



which produces acetaldehyde. Recent *ab initio* calculations showed that the dominant reaction channel is the one that produces ethenol

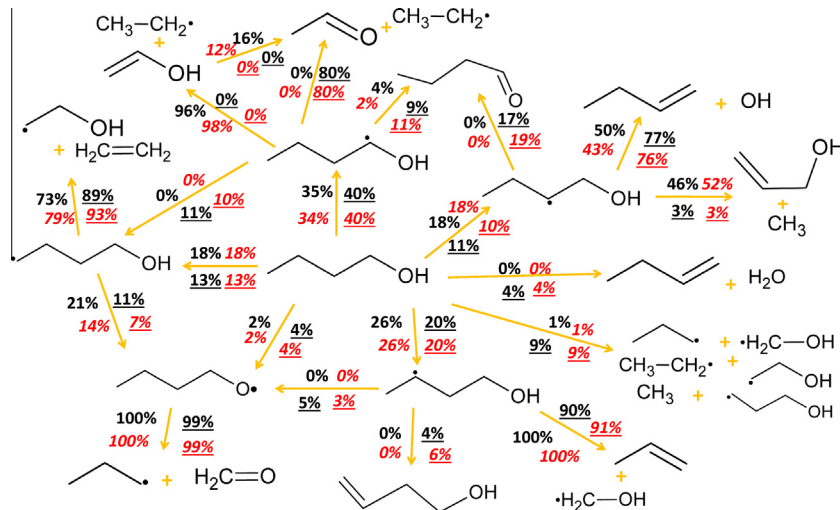


Fig. 14. Fuel cracking path of the stoichiometric 1-D planar flame of *n*-butanol at 1 and 5 atm, calculated using the S- and R-mechanisms. The numbers indicate the conversion percentage (regular: 1 atm with air as oxidizer; italic: 5 atm with 13%O₂–38.1%Ar–48.9%He as oxidizer; text without underline: S-mechanism; text with underline: R-mechanism).

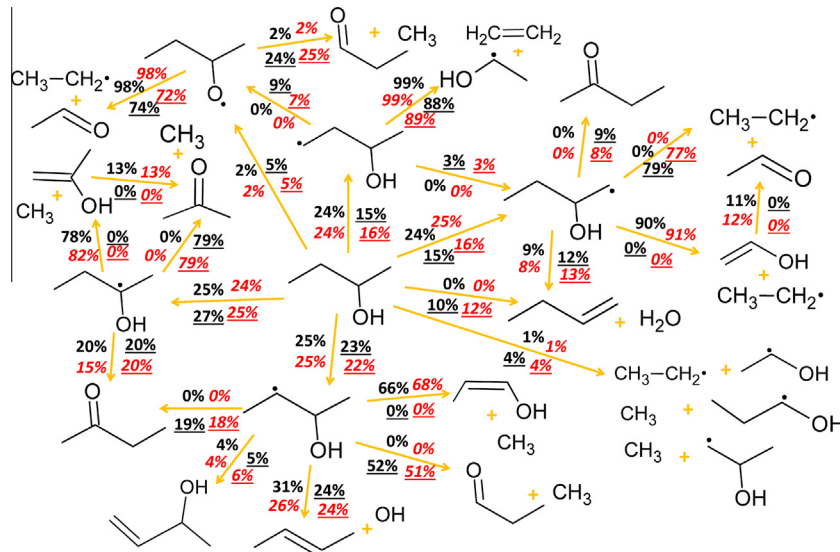


Fig. 15. Fuel cracking path of the stoichiometric 1-D planar flame of *s*-butanol at 1 and 5 atm, calculated using the S- and R-mechanisms. The numbers indicate the conversion percentage (regular: 1 atm with air as oxidizer; italic: 5 atm with 13%O₂–38.1%Ar–48.9%He as oxidizer; text without underline: S-mechanism; text with underline: R-mechanism).

[33]. While enols are unstable and readily undergo enol-keto tautomerization producing aldehydes or ketones, the reaction is shown to have high energy barrier and thus is slow in comparison to other reactions, such as the H abstraction of enols [34]. Therefore the difference of replacing enols by aldehydes or ketones is not negligible. The conversion percentage from ethenol to acetaldehyde computed using the S-mechanism is only 12–16%. The second difference between the two mechanisms is that the dominant reaction pathway of fuel radicals, *i.e.* the β-scission reactions at C–C or C–O bond, has higher conversion percentage values in the S-mechanism than those in the R-mechanism. In other words, in the R-mechanism the dominant β-scission pathways are attenuated by other pathways, such as isomerization and β-scission reactions at the C–H bond. For example, 100% of 3-hydroxybutyl radical in the S-mechanism produces propene and CH₂OH radical, while in the R-mechanism it is also converted into *n*-butoxy via isomerization and 3-buten-1-ol (CH₂=CHCH₂CH₂OH) via the β-scission reaction

at the C–H bond. The only fuel radical isomerization reaction that is not negligible in the S-mechanism is the one between 3-hydroxybutyl radical and *n*-butoxy. In addition, in the R-mechanism the direct fuel decomposition and water elimination also have higher conversion percentages than those in the S-mechanism.

Similar to *n*-butanol, H abstraction reactions converted most of *s*-butanol into hydroxybutyl radicals of *s*-butanol and a small portion into *s*-butoxy radical, as shown in Fig. 15. There are also four hydroxybutyl radicals for *s*-butanol: 1-hydroxybutyl, 2-hydroxybutyl, 3-hydroxybutyl and *m*-hydroxybutyl. They mostly undergo β-scission producing smaller alkenes, enols, aldehydes and ketones species. Different from *n*-butanol which only produces straight-chain fragments, *s*-butanol flames also have branched intermediates, such as iso-propenol (iC₃H₅OH), acetone (CH₃COCH₃) and 2-butanone (C₂H₅COCH₃). The differences between the two kinetic models shown for the case of *n*-butanol are also the same for *s*-butanol. In the R-mechanism, enols produced from fuel radical

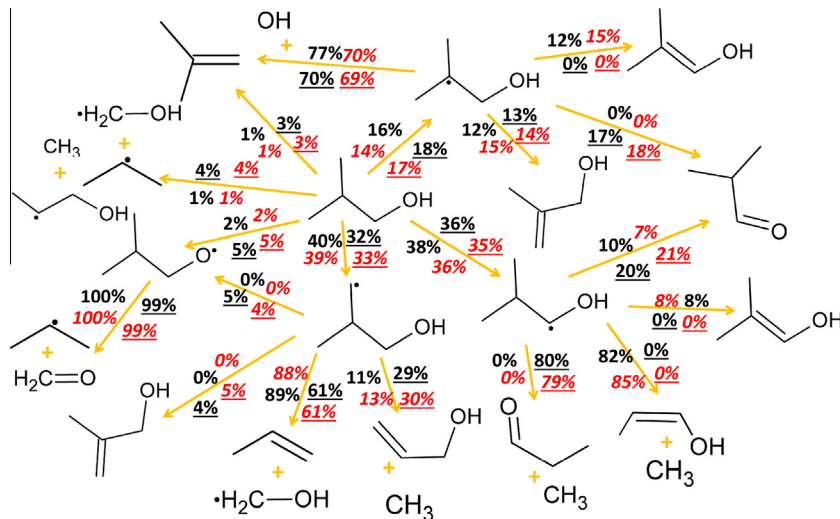


Fig. 16. Fuel cracking path of the stoichiometric 1-D planar flame of *i*-butanol at 1 and 5 atm, calculated using the S- and R-mechanisms. The numbers indicate the conversion percentage (regular: 1 atm with air as oxidizer; italic: 5 atm with 13% O₂–38.1% Ar–48.9% He as oxidizer; text without underline: S-mechanism; text with underline: R-mechanism).

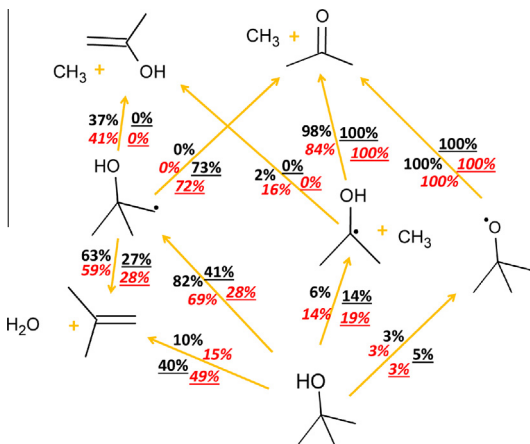


Fig. 17. Fuel cracking path of the stoichiometric 1-D planar flame of *t*-butanol at 1 and 5 atm, calculated using the S- and R-mechanisms. The numbers indicate the conversion percentage (regular: 1 atm with air as oxidizer; italic: 5 atm with 13% O₂–38.1% Ar–48.9% He as oxidizer; text without underline: S-mechanism; text with underline: R-mechanism).

β -scission reactions are replaced by aldehydes or ketones. For example, in the decomposition of m-hydroxybutyl, 1-hydroxybutyl and 2-hydroxybutyl, the products ethenol, *iso*-propenol and 1-propen-1-ol ($\text{CH}_3\text{CH}=\text{CHOH}$) are replaced by acetaldehyde, acetone and propanal ($\text{C}_2\text{H}_5\text{CHO}$). Similar to *n*-butanol, the direct fuel decomposition, water elimination and fuel radical isomerization reactions in the *s*-butanol flames also have higher conversion percentages in the R-mechanism than those in the S-mechanism. In addition, we notice that the R-mechanism does not distinguish isomers of some intermediate species. For example, 1-butene and 2-butene are treated as one species NC4H8 in R-mechanism. Furthermore, 3-buten-1-ol ($\text{CH}_2=\text{CHCH}_2\text{CH}_2\text{OH}$), 2-methyl-2-propen-1-ol ($\text{CH}_2=\text{C}(\text{CH}_3)\text{CH}_2\text{OH}$) and 3-buten-2-ol ($\text{CH}_2=\text{CHCH}(\text{CH}_3)\text{OH}$), which respectively come from the decomposition of hydroxybutyl radicals of *n*-butanol, *s*-butanol and *i*-butanol, are also treated as a single species, C₄H₇OH, in the R-mechanism.

The initial cracking of *i*-butanol follows similar steps as *n*-butanol and *s*-butanol, although the resulting fuel fragments are different. There are three hydroxybutyl radical for *i*-butanol:

1-hydroxybutyl, 2-hydroxybutyl and 3-hydroxybutyl, which again are the main products of H-abstraction of the fuel, leaving *iso*-butoxy radical only a small percentage. The decomposition of 1-hydroxybutyl and 3-hydroxybutyl radical produces mostly straight-chain intermediates, such as propene and propenols, while 2-hydroxybutyl radical produces all branched intermediate species that contain a C₄ alkenyl group, such as *iso*-butene, 2-methyl-1-propen-1-ol ((CH_3)₂C=CHOH) and 2-methyl-2-propen-1-ol. From Fig. 16 it is seen that for *i*-butanol the R-mechanism also directly replaces enols in the products of hydroxybutyl radical decomposition by aldehydes or ketones, such as 1-propen-1-ol replaced by propanal in the decomposition reaction of 1-hydroxybutyl *i*-butanol radical. Similar to *n*-butanol and *s*-butanol, direct fuel decomposition, water elimination and fuel radical isomerization reactions have higher conversion percentages in the R-mechanism by than that in the S-mechanism.

Lastly, for *t*-butanol, it is seen from Fig. 17 that the reaction path is much simpler than those of the other butanol isomers. Since the ternary C atom in the *t*-butanol molecule does not have an H atom connected to it and the three other C atoms are symmetric, there is only one *t*-butanol hydroxybutyl radical: (CH_3)₂(CH₂)COH. The dominant path of the H-abstraction reaction of *t*-butanol is the one producing (CH_3)₂(CH₂)COH; only a small portion produces *tert*-butoxyl radical ((CH_3)₃CO). In addition, *t*-butanol can also undergo water elimination reaction which produces *iso*-butene, or directly decompose into CH₃ and (CH_3)₂COH radical. Similar to other isomers, the water elimination reaction and direct fuel decomposition reaction have much higher conversion percentages in the R-mechanism than in the S-mechanism. The (CH_3)₂(CH₂)COH radical undergoes two β -scission reactions producing *iso*-butene and *iso*-propenol respectively. In the R-mechanism there is no *iso*-propenol species, which is replaced by acetone directly. The (CH_3)₂COH radical mostly undergoes β -scission producing acetone, with a small portion of it produces *iso*-propenol in the S-mechanism. In any case, the reaction path of *t*-butanol has to go through *iso*-butene, *iso*-propenol or acetone.

In general, we do not see a strong pressure effect between 1 atm and 5 atm on the initial fuel cracking pathways and conversion rates. For most of the reactions in the reaction path of *n*-butanol, *s*-butanol and *i*-butanol, the conversion percentages at 5 atm are very close to the values at 1 atm. The pressure effect on the reaction path of *t*-butanol is a little stronger. From Fig. 17, it is seen that

with both mechanisms increasing pressure tends to reduce the conversion percentages of H abstraction reactions while increasing the percentages of water elimination and fuel decomposition reactions. In the S-mechanism, increasing pressure also causes $(\text{CH}_3)_2\text{COH}$ radical to decompose more *iso*-propenol.

4.4. Relation to bond energies

From the above reaction path analysis for all isomers, it can be concluded that while *n*-butanol all cracks into straight-chain species (oxygenated or not), *s*-butanol, *i*-butanol and *t*-butanol crack into significantly more branched species. Specifically, in the flames of *i*-butanol a significant amount of fuel is converted to *iso*-butene and oxygenated species with similar branched carbon structure, such as 2-methyl-2-propen-1-ol. *iso*-butene is a notably stable species and has slow flame speeds as noted in many previous studies [31,35]. In the *s*-butanol flame, *iso*-butene is not formed; however, there are considerably more acetone (CH_3COCH_3) and *iso*-propenol ($\text{iC}_3\text{H}_5\text{OH}$). As shown in [15,36], acetone and *iso*-propenol can exchange through tautomerization reaction or isomerization reactions with radical, and they both are relatively stable intermediate species. This therefore explains the lower flame speed of *s*-butanol relative to *n*-butanol. Finally, in *t*-butanol flames all the fuel is converted to branched species: *iso*-butene, acetone and *iso*-propenol. Therefore the combined effect of the low reactivity of these three branched species causes *t*-butanol to have the lowest flame speeds.

It is noted that many previous studies have shown that branched hydrocarbons has slower flame speed compared to their straight chain counterparts, such as *iso*-butane versus *n*-butane [24,35], *iso*-butene versus 1-butene and 2-butene [24], and *iso*-octane versus *n*-octane [18,37]. Now we see that this rule can also be applied for alcohols, which contains not only C–C, C–H bonds but also C–O and O–H bond. The fundamental reason for this similarity lies in the bond energies. The calculation in [6] shows the following ordering of bond dissociate energies in the butanol fuel molecules: O–H bond (104–107 kcal/mol) > terminal C–H bond (100–103 kcal/mol) > inner C–H bond (97–99 kcal/mol) > C–O bond (93–96 kcal/mol) > C–C bond (85–90). For hydroxybutyl radicals, the bond energies at the β position will be different but the ordering remains approximately. It is seen that the C–O bond has similar bond energy as the C–C bond, while the O–H bond has similar bond energy as the C–H bond. In hydrocarbon fuels, β scission at C–C is usually the dominant reaction path because it has lower bond energy than that of the C–H bond. Whereas for alcohols β scission at both C–C and C–O are the dominant pathways because they have similar bond energies, which in turn are lower than the energies of C–H bond and O–H bond. In other words, in high temperature chemistry where H abstraction followed by β scission is the dominant reaction pathway, the role of the O atom is similar to the C atom when we consider the extent of branching of a fuel. In this sense, if we consider the chain structure formed by the C–C and C–O bonds, only *n*-butanol has the straight chain structure, whereas *s*-butanol, *i*-butanol and *t*-butanol all crack into various amount of branched intermediate species, which are kinetically more stable.

5. Conclusions

Using expanding spherical flames, laminar flame speeds and Markstein lengths for *n*-butanol, *s*-butanol, *i*-butanol and *t*-butanol were determined at pressures from 1 to 5 atm over a wide range of equivalence ratios. Results at all pressures show that *n*-butanol has the highest flame speed, followed by *s*-butanol and *i*-butanol, and then *t*-butanol; with the flame speeds of *s*-butanol and *i*-butanol

being almost the same. This ordering of flame speeds also agrees with measurements of Veloo and Egolfopoulos [3] at 1 atm, recognizing nevertheless that their values are slightly higher than the present data for *n*-butanol, *s*-butanol and *i*-butanol, particularly for the lean conditions. The computed flame speeds using the S-mechanism, by Sarathy et al. [15], have satisfactory agreement with the present data for all fuels at all pressures, with a slight over-prediction for *n*-butanol and *s*-butanol. The agreement with the computed flame speeds using the R-mechanism, by Ranzi et al. [16], is less satisfactory: the model over predicts the flame speeds of *n*-butanol, *s*-butanol, *i*-butanol and *t*-butanol at 1 atm, while under predicts the flame speeds of *n*-butanol and *s*-butanol at 5 atm.

Measurements show that the Markstein lengths of all butanol isomers have similar values at 1 and 2 atm, whereas at 5 atm with oxygen–helium–argon mixture as the oxidizer the Markstein lengths of *n*-butanol are considerably lower than others. However, we have demonstrated that this lower Markstein length for *n*-butanol is caused by its reduced flame thickness, which in turn is caused by its higher flame speed. The Markstein numbers (Markstein lengths scaled by flame thickness) of *n*-butanol are actually similar to those of other isomers. This indicates that the butanol isomers have similar nonequidiffusive properties when subjected to aerodynamic stretching.

Computational analysis showed that the difference in the adiabatic temperatures among different butanol isomers only causes approximately 20% difference in their flame speeds, implying that kinetics is the main reason for the difference in the flame speeds. To further investigate the cause, rate constant and sensitivity analysis, as well as reaction path analysis were performed using both the S- and R-mechanisms. Comparison of the two mechanisms revealed that the major difference in the fuel cracking path lies in the products of some β -scission reactions and the weighting of H-abstraction/ β -scission pathways versus other pathways such as fuel decomposition and water elimination. In addition, the R-mechanism also replaces enols produced from β -scission reactions by aldehydes or ketones.

Reaction path analysis showed that *s*-butanol, *i*-butanol and *t*-butanol all crack into some amount of branched intermediate species, such as *iso*-butene, acetone and *iso*-propenol, which are more stable as compared to the straight chain counterpart and thus reduce the flame speed. This means the general rule that branched fuels have lower flame speed also applies to alcohols. We found that this generality is due to the fact that in alcohols C–O has similar bond energy as that of the C–C bond while O–H has similar bond energy as that of the C–H bond. Consequently the role of an O atom is similar to a C atom when we consider the extent of branching of a fuel.

Acknowledgments

This work was supported by the Combustion Energy Frontier Research Center, an Energy Frontier Research Center funded by the US Department of Energy, Office of Basic Energy Sciences under Award Number DESC0001198. The authors thank Professor Mani Sarathy for his help in using the S-mechanism, Professor Alessio Frassoldati his help in using the R-mechanism and the OpenSMOKE code, and Professor Yiguang Ju and Roe Burrell for their help in the use of the PLOG Chemkin code.

References

- [1] P.S. Nigam, A. Singh, Prog. Energy Combust. Sci. 37 (2011) 52–68.
- [2] S.M. Sarathy, M.J. Thomson, C. Togbé, P. Dagaout, F. Halter, C. Mounaim-Roussel, Combust. Flame 156 (2009) 852–864.
- [3] P.S. Veloo, F.N. Egolfopoulos, Proc. Combust. Inst. 33 (2011) 987–993.
- [4] W. Liu, A.P. Kelley, C.K. Law, Proc. Combust. Inst. 33 (2011) 995–1002.

- [5] X. Gu, Z. Huang, Q. Li, C. Tang, *Energy Fuels* 23 (2009) 4900–4907.
- [6] X. Gu, Z. Huang, S. Wu, Q. Li, *Combust. Flame* 157 (2010) 2318–2325.
- [7] X. Gu, Q. Li, Z. Huang, *Combust. Sci. Technol.* 183 (2011) 1360–1375.
- [8] X. Gu, Q. Li, Z. Huang, N. Zhang, *Energy Convers. Manage.* 52 (2011) 3137–3146.
- [9] M.R. Harper, K.M. Van Geem, S.P. Pyl, G.B. Marin, W.H. Green, *Combust. Flame* 158 (2011) 16–41.
- [10] S. Vranckx, K.a. Heufer, C. Lee, H. Olivier, L. Schill, W.a. Kopp, et al., *Combust. Flame* 158 (2011) 1444–1455.
- [11] G. Black, H.J. Curran, S. Pichon, J.M. Simmie, V. Zhukov, *Combust. Flame* 157 (2010) 363–373.
- [12] N. Hansen, M.R. Harper, W.H. Green, *Phys. Chem. Chem. Phys.* 13 (2011) 20262–20274.
- [13] K.M. Van Geem, S.P. Pyl, G.B. Marin, M.R. Harper, W.H. Green, *Ind. Eng. Chem. Res.* 49 (2010) 10399–10420.
- [14] J.T. Moss, A.M. Berkowitz, M.a. Oehlschlaeger, J. Biet, V. Warth, P.-A. Glaude, et al., *J. Phys. Chem. A* 112 (2008) 10843–10855.
- [15] S.M. Sarathy, S. Vranckx, K. Yasunaga, M. Mehl, P. Oßwald, W.K. Metcalfe, et al., *Combust. Flame* 159 (2012) 2028–2055.
- [16] E. Ranzi, A. Frassoldati, R. Grana, A. Cuoci, T. Faravelli, A.P. Kelley, et al., *Progr. Energy Combust. Sci.* (2011).
- [17] A.P. Kelley, A.J. Smallbone, D.L. Zhu, C.K. Law, Experimental measurement of n-pentane flame speeds at elevated pressures and temperatures, in: 6th US National Combustion Meeting, 2009.
- [18] A.P. Kelley, A.J. Smallbone, D.L. Zhu, C.K. Law, *Proc. Combust. Inst.* 33 (2011) 963–970.
- [19] F. Wu, A.P. Kelley, C.K. Law, *Combust. Flame* 159 (2012) 1417–1425.
- [20] A.P. Kelley, J.K. Bechtold, C.K. Law, Confined propagation of premixed flames, in: 7th US National Combustion Meeting, 2011.
- [21] A.P. Kelley, G. Jomaas, C.K. Law, *Combust. Flame* 156 (2009) 1006–1013.
- [22] M.P. Burke, Z. Chen, Y. Ju, F.L. Dryer, *Combust. Flame* 156 (2009) 771–779.
- [23] Z. Chen, M.P. Burke, Y. Ju, *Proc. Combust. Inst.* 32 (2009) 1253–1260.
- [24] A.P. Kelley, Dynamics of expanding flames, PhD thesis, Princeton University, 2011.
- [25] R.J. Kee, J.F. Grcar, M.D. Smooke, J.A. Miller, E. Meeks, Premix: a Fortran program for modeling steady laminar one-dimensional premixed flames. Sandia report 85–8240, 1985.
- [26] X.L. Gou, J.A. Miller, W.T. Sun, Y. Ju, Implementation of PLOG function in Chemkin II and III, 2011.
- [27] A. Cuoci, A. Frassoldati, T. Faravelli, E. Ranzi, Open SMOKE: numerical modeling of reacting systems with detailed kinetic mechanisms, in: XXXIV Meeting of the Italian Section of the Combustion Institute, Rome, Italy, 2011.
- [28] C. Ji, E. Dames, Y.L. Wang, H. Wang, F.N. Egolfopoulos, *Combust. Flame* 157 (2010) 277–287.
- [29] C. Ji, E. Dames, B. Sirjean, H. Wang, F.N. Egolfopoulos, *Proc. Combust. Inst.* 33 (2011) 971–978.
- [30] H.H. Kim, S.H. Won, J. Santner, Z. Chen, Y. Ju, *Proc. Combust. Inst.* 34 (2013) 929–936.
- [31] C. Ji, S.M. Sarathy, P.S. Veloo, C.K. Westbrook, F.N. Egolfopoulos, *Combust. Flame* 159 (2012) 1426–1436.
- [32] X. You, F.N. Egolfopoulos, H. Wang, *Proc. Combust. Inst.* 32 (2009) 403–410.
- [33] P. Zhang, S.J. Klippenstein, C.K. Law, Ab initio kinetics for the decomposition of α -hydroxybutyl radicals of n-butanol, in: Fall Technical Meeting of the Eastern States Section of the Combustion Institute, 2011.
- [34] G. Silva, C. Kim, J.W. Bozzelli, *J. Phys. Chem. A* 110 (2006) 7925–7934.
- [35] S.G. Davis, C.K. Law, *Combust. Sci. Technol.* 140 (1998) 427–449.
- [36] J.K. Lefkowitz, J.S. Heyne, S.H. Won, S. Dooley, H.H. Kim, F.M. Haas, et al., *Combust. Flame* 159 (2012) 968–978.
- [37] A.P. Kelley, W. Liu, Y.X. Xin, A.J. Smallbone, C.K. Law, *Proc. Combust. Inst.* 33 (2011) 501–508.